Semiautomatic registration of 3D transabdominal ultrasound images for patient repositioning during postprostatectomy radiotherapy

Benoît Presles[a)]
Université de Lyon, CREATIS, CNRS UMR5220, Inserm U1044, INSA-Lyon, Université Lyon 1, Lyon F-69621, France and Léon Bérard Cancer Center, Université de Lyon, Lyon F-69373, France

Marie Fargier-Voiron
Université de Lyon, CREATIS, CNRS UMR5220, Inserm U1044, INSA-Lyon, Université Lyon 1, Lyon F-69621, France

Marie-Claude Biston
Léon Bérard Cancer Center, Université de Lyon, Lyon F-69373, France

Rod Lynch
The Andrew Love Cancer Centre, University Hospital Geelong, Geelong 3220, Australia

Alexandre Munoz
Léon Bérard Cancer Center, Université de Lyon, Lyon F-69373, France

Hervé Liebgott
Université de Lyon, CREATIS, CNRS UMR5220, Inserm U1044, INSA-Lyon, Université Lyon 1, Lyon F-69621, France

Pascal Pommier
Léon Bérard Cancer Center, Université de Lyon, Lyon F-69373, France

Simon Rit and David Sarrut
Université de Lyon, CREATIS, CNRS UMR5220, Inserm U1044, INSA-Lyon, Université Lyon 1, Lyon F-69621, France and Léon Bérard Cancer Center, Université de Lyon, Lyon F-69373, France

(Received 19 February 2014; revised 31 October 2014; accepted for publication 3 November 2014; published 2 December 2014)

Purpose: The aim of the present work is to propose and evaluate registration algorithms of three-dimensional (3D) transabdominal (TA) ultrasound (US) images to setup postprostatectomy patients during radiation therapy.
Methods: Three registration methods have been developed and evaluated to register a reference 3D-TA-US image acquired during the planning CT session and a 3D-TA-US image acquired before each treatment session. The first method (method A) uses only gray value information, whereas the second one (method B) uses only gradient information. The third one (method C) combines both sets of information. All methods restrict the comparison to a region of interest computed from the dilated reference positioning volume drawn on the reference image and use mutual information as a similarity measure. The considered geometric transformations are translations and have been optimized by using the adaptive stochastic gradient descent algorithm. Validation has been carried out using manual registration by three operators of the same set of image pairs as the algorithms. Sixty-two treatment US images of seven patients irradiated after a prostatectomy have been registered to their corresponding reference US image. The reference registration has been defined as the average of the manual registration values. Registration error has been calculated by subtracting the reference registration from the algorithm result. For each session, the method has been considered a failure if the registration error was above both the interoperator variability of the session and a global threshold of 3.0 mm.
Results: All proposed registration algorithms have no systematic bias. Method B leads to the best results with mean errors of −0.6, 0.7, and −0.2 mm in left–right (LR), superior–inferior (SI), and anterior–posterior (AP) directions, respectively. With this method, the standard deviations of the mean error are of 1.7, 2.4, and 2.6 mm in LR, SI, and AP directions, respectively. The latter are inferior to the interoperator registration variabilities which are of 2.5, 2.5, and 3.5 mm in LR, SI, and AP directions, respectively. Failures occur in 5%, 18%, and 10% of cases in LR, SI, and AP directions, respectively. 69% of the sessions have no failure.
Conclusions: Results of the best proposed registration algorithm of 3D-TA-US images for post-prostatectomy treatment have no bias and are in the same variability range as manual registration. As the algorithm requires a short computation time, it could be used in clinical practice

provided that a visual review is performed.
[http://dx.doi.org/10.1118/1.4901642]

Key words: postprostatectomy, radiotherapy, registration, ultrasound

1. INTRODUCTION

Prostatic bed radiation therapy (RT) is a common practice after radical prostatectomy for either adjuvant RT or salvage RT.[1] The location of the prostatic bed can vary from session to session[2] due in particular to changes in the surrounding structures from rectal and bladder filling. Therefore, patient positioning based on the location of the prostatic bed before each radiation session is of major importance. The use of a three-dimensional (3D) transabdominal (TA) ultrasound (US) system could be a better alternative to x-ray-based modalities since US-based imaging offers better tissue contrast[3] and is noninvasive and nonirradiating, avoiding the associated risks for the patient.[4] Three different ultrasound image guided radiation therapy (IGRT) devices have been commercialized over the past 15 years, BAT® (Nomos, Pittsburgh, PA, USA),[5] SonArray® (Varian, Palo Alto, CA, USA),[6] and Clarity® (formerly named Restitu®) (Elekta, Stockholm, Sweden).[7] Unlike the other systems, the latter uses an intramodality approach based on the comparison of 3D-TA-US images acquired at each treatment session, to a reference 3D-TA-US image acquired during the planning CT acquisition. In clinical practice, a reference contour, drawn onto the reference US image, is manually translated on the daily US image in order to register the delineated structure and therefore retrieve the potential target displacement. For the post-prostatectomy localization, very few anatomical structures are visible on ultrasound unlike other treatment sites. Therefore, the recommended surrogate for prostatic bed positioning is the bladder neck[8,9] which is defined by the bladder walls, except in the superior direction (Fig. 1). Several US/US registration algorithms, either intensity-based or feature-based, have been proposed in the literature and successfully applied to various sites such as breast,[10,11] liver,[12–16] kidney,[16] heart,[15–22] or prostate.[23–25] However, to our knowledge, no automated approach has been investigated for the registration of 3D-TA-US/3D-TA-US postprostatectomy images. In this paper, the authors evaluate and compare quantitatively three different registration algorithms on a set of 62 3D-TA-US postprostatectomy images from seven patients.

2. MATERIAL AND METHODS

2.A. The US process for postprostatectomy repositioning

The US-IGRT system used to acquire the US images is the Clarity® device that has already been described elsewhere.[7] It is based on a TA probe that uses a position sensor via optical tracking equipment (an infrared camera). For each acquisition, several hundred 2D-US slices are acquired during a probe sweep and are merged in a 3D image, based on their spatial location.[26] The tracking system tracks the probe in its own coordinate system but refers to the room coordinate system defined by the room lasers thanks to a calibration.[27] During the CT session, a reference 3D-TA-US image, denoted by US_{ref}, is acquired with the patient in the same position as for the CT acquisition. The CT image is already expressed in the room basis but the origin of CT coordinate system is not necessarily the lasers intersection, i.e., the simulation isocenter. The location of the simulation isocenter is determined by using radio-opaque fiducial markers that are placed at the location of the patient skin marks and aligned with the room lasers. These markers can then be identified on the CT image. The US_{ref} and CT images are therefore both expressed in the room coordinate system and can be superimposed directly without the need of an additional registration as illustrated in Fig. 1.

During the planning phase, the clinical target volume (CTV) is delineated on the CT image. For postprostatectomy irradiation, it includes the bladder neck, the urethra-vesical anastomosis, the neurovascular bundles, the anastomosis, and the urethral axis as recommended by Poortmans *et al.*[28] The Clarity workflow also requires an expert to manually delineate a reference positioning volume (RPV) on the US_{ref} image because organ volumes appear differently according to the used modality.[3] Since US imaging allows for differentiation between soft tissues, enabling an accurate visualization of the bladder wall, the RPV contoured on the US_{ref} image is the bladder neck. To delineate this volume, the entire bladder is contoured on the US_{ref} image, then the volume is cropped superiorly leaving only the bladder neck (Fig. 1).

Over the treatment course, a daily 3D-TA-US image, denoted by US_{daily}, is acquired at the beginning of each treatment session fraction, and the patient is setup by registering the RPV onto the US_{daily} image. As there is currently no automatic registration algorithm available, the registration is entirely performed manually by trained radiation therapists. RPV is shifted only with translations to match the reference image.

Data from seven patients who underwent postprostatectomy RT and for which the US-IGRT system was used, have been retrospectively analyzed. In total, 62 US_{daily} images (5–15 images per patient) have been registered to their corresponding US_{ref} image.

2.B. 3D-TA-US/3D-TA-US registration algorithms

As explained in Sec. 2.A, repositioning using the clarity system involves two steps. The first step is the manual segmentation of a RPV and the second step is the manual registration of the reference and daily images. To date, both steps are manual. The aim of this study is to propose an automatic method for the second step.

To do so, three methods based on mutual information (MI)[29] have been tested. Indeed, MI is a widespread similarity

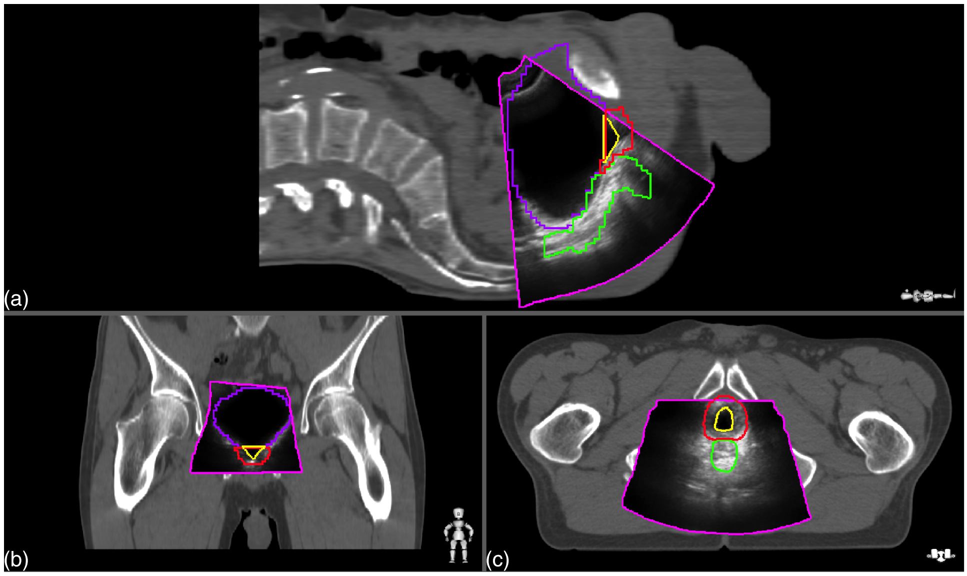

FIG. 1. Example of a 3D transabdominal reference ultrasound image superimposed on the planning CT image in sagittal (a), coronal (b), and axial (c) views. The CT contours of the CTV, rectum, and bladder are in red (the smallest CT contour), green (the medium CT contour), and purple (the largest CT contour), respectively. The RPV contoured on the US image, i.e., the bladder neck, is in yellow (the smallest US contour) and the US cone in pink (the largest US contour).

measure for monomodal and multimodal registration[30] and has been used successfully to register ultrasound images.[17,31]

The first method, denoted *method A*, directly applies MI on US_{ref} and US_{daily} images without any preprocessing. However, gray value information in US images may not be relevant in comparison with other modalities because of the presence of speckle noise and considering gradient information can improve the registration.[32] Thus, the second method, denoted *method B*, computes MI between the gradient magnitude of the US_{ref} and US_{daily} images. The third method, denoted *method C*, combines gray value and gradient information. US_{ref} and US_{daily} images are preprocessed by calculating their *importance images* as proposed by Foroughi *et al.*[13] and Kaar *et al.*[25] The importance image is defined as a linear combination of the original gray level image, its gradient magnitude image and its Laplacian image. The relative weights between each component are chosen as suggested by Kaar *et al.*[25] and are equal to $1/4$, $1/2$, and $1/4$ for the gray level, gradient, and Laplacian images, respectively. One can notice that the methods A and B can be seen as a variation of the method C, the relative weights between each component being equal to 1, 0, 0 and 0, 1, 0 for the gray level, gradient, and Laplacian images, respectively.

The US_{ref} and US_{daily} images are considered as the fixed and moving images, respectively, as the RPV is defined on the US_{ref} image. For each image, the foreground, i.e., the conic US field-of-view, is detected and used in the computation of the MI to consider only pairs of pixels that are in the conic US field-of-view of the two images. The registration is further limited to the tissues around the RPV to only consider the target volume displacement and to improve the algorithm robustness by restricting the registration to a region that has little anatomical variability. A region of interest (ROI) is defined on the fixed image as the intersection between the RPV volume dilated with a ball of radius r mm structuring element and the conic mask (Fig. 2).

The geometric transformation is limited to a 3D translation. The three parameters are optimized with the adaptive stochastic gradient descent algorithm.[33] The MI is computed on sets of 5000 voxels stochastically selected from the ROI at each iteration. The stopping criteria of the optimization algorithm

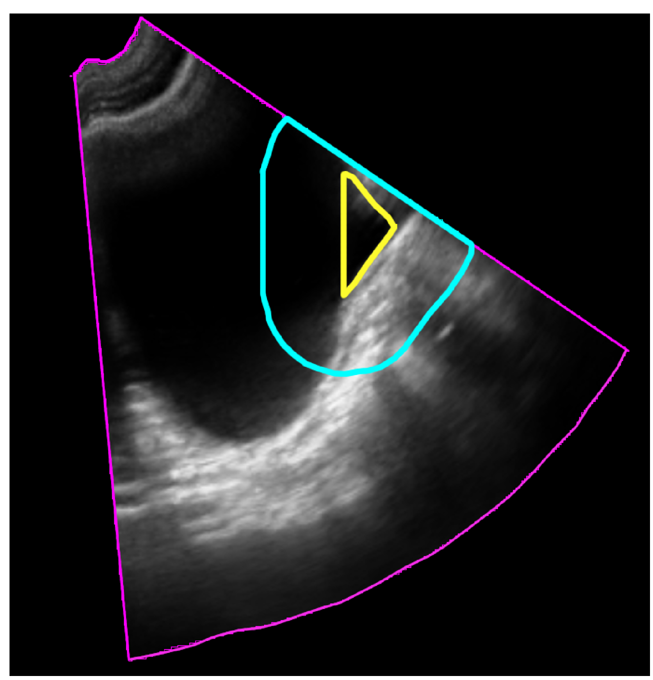

FIG. 2. Sagittal view of the ROI used to locally register the tissues around the RPV. The ROI (the medium contour in blue) is defined as the intersection between the RPV volume (the smallest contour in yellow) dilated with a ball of radius r mm structuring element and the conic mask (the largest contour in pink).

is the number of iterations fixed at 2000. The whole process is performed using the elastix toolbox,[34] which is based on the Insight Segmentation and Registration Toolkit (ITK).[35]

2.C. Reference registration

Three trained operators have manually registered all 62 sessions using the Clarity® system. Registrations have been performed in a blind manner, the operators did not see the registrations of the others. The obtained translations are denoted $T_{p,s,o}$ with p, s, and o being the patient, session, and operator indices, respectively. Shifts are expressed in terms of left–right (LR), anterior–posterior (AP), and superior–inferior (SI) directions. From these values, the interoperator variability IOV has been computed. Moreover, to see if the variability between the operators is more session specific or patient specific, the root mean square (RMS) of the intersession variability of the operator variability, and the interpatient variability of the RMS of the operator variability have been computed, respectively. These variabilities of variabilities are denoted intersession interoperator variability (ISIOV) and interpatient interoperator variability (IPIOV), respectively (Table I).

If the session standard deviation $\sigma_{p,s}$ of the translations $T_{p,s,o}$ between the three operators was above a threshold of 5 mm, the three operators were asked to redo their registrations. The obtained reviewed translations are denoted $T'_{p,s,o}$ and have only been used to calculate *a reference registration*. The latter is defined as the average translation over the operators, $\mu'_{p,s} = 1/3 \sum_{o=1}^{3} T'_{p,s,o}$. The IOV, ISIOV, and IPIOV are calculated with the original translation $T_{p,s,o}$ values and not with the reviewed values.

2.D. Errors quantification

The three methods A, B, and C have been evaluated on the same dataset. The performance of the registration has been evaluated by calculating for each session the *misalignment vector* $MV_{p,s}$ defined as the difference between the translation $T_{p,s,a}$ found by the algorithm a and the reference registration $\mu'_{p,s}$: $MV_{p,s} = T_{p,s,a} - \mu'_{p,s}$. The length of the misalignment vector $LMV_{p,s}$ has also been calculated, $LMV_{p,s} = \|T_{p,s,a} - \mu'_{p,s}\|_2$, where $\|.\|_2$ denotes the L_2 norm. The weighted average of the misalignment vectors MV and the weighted average of the misalignment vector lengths LMV ($MV = 1/P \sum_{p=1}^{P} 1/S_p \sum_{s=1}^{S_p} MV_{p,s}$, $LMV = 1/P \sum_{p=1}^{P} 1/S_p \sum_{s=1}^{S_p} LMV_{p,s}$, where S_p denotes the number of session of the patient p and P denotes the total number of patient) have been calculated to get mean registration error values.

To quantify the accuracy and the precision of the algorithm session by session, the absolute error, i.e., $|MV_{p,s}|$, and the error relative to the operator variability, i.e., $|MV_{p,s}|/\sigma_{p,s}$, have jointly been considered to detect algorithm failures. For each session, the registration is considered as a failure if the absolute value of $MV_{p,s}$ is both above a threshold of 3.0 mm, which is the order of magnitude of the IOV, and above the session standard deviation $\sigma_{p,s}$ value. In these cases, the registration value is both far from the reference registration and above the variability of the registration made by the three operators. Results are presented in a 2D histogram h constructed as follows: $\forall (i,j) \in \mathbb{N}\times\mathbb{N}, h(i+0.5, j+0.5) = \mathrm{Card}\{MV_{p,s} | i \le |MV_{p,s}|/\sigma_{p,s} < i+1 \; and \; j \le |MV_{p,s}| < j+1\} / \sum_{k\in\mathbb{N}} \sum_{l\in\mathbb{N}} h(k,l)$. For example, the first square of the histogram ($i = j = 0$), counts the number of $|MV_{p,s}|$ values that are both inferior to 1 mm and inferior to $\sigma_{p,s}$, in which case the registration error is intrinsically small and inferior to the operator variability. The $|MV_{p,s}|$ values in the first column of the histogram ($i = 0$) are error values that can be intrinsically important but are still lower than the operator variability and therefore cannot be considered as failures since the reference value has a large variability. Likewise, the $|MV_{p,s}|$ values in the first rows of the histogram ($j < 3.0$ mm) are small error values and cannot be considered as failures even if the error relative to the operator variability $|MV_{p,s}|/\sigma_{p,s}$ is high. Indeed, in these cases, the three operators agree, i.e., $\sigma_{p,s}$ approaches zero, and therefore $|MV_{p,s}|/\sigma_{p,s}$ approaches infinity.

3. RESULTS

3.A. Manual reference registration

Table II shows the interoperator IOV, intersession ISIOV, and interpatient IPIOV variabilities in all directions. All variabilities are larger in AP direction and minimum in SI direction. Registration difficulties are more session-dependent than patient-dependent since ISIOV is larger than IPIOV for all directions.

3.B. Automatic registration results

Figure 3 shows the average of the misalignment vector lengths LMV as a function of the radius r for the methods A

TABLE I. Interoperator, intersession, and interpatient variabilities.

Variability	Abbreviation	Equation
Interoperator	IOV	$\sqrt{1/P \sum_{p=1}^{P} \mathrm{rms}_{\sigma_p}^2}$ with $\mathrm{rms}_{\sigma_p} = \sqrt{1/S_p \sum_{s=1}^{S_p} \sigma_{p,s}^2}$
Intersession	ISIOV	$\sqrt{1/P \sum_{p=1}^{P} 1/S_p \sum_{s=1}^{S_p} (\sigma_{p,s} - \overline{\sigma_p})^2}$ with $\overline{\sigma_p} = 1/S_p \sum_{s=1}^{S_p} \sigma_{p,s}$
Interpatient	IPIOV	$\sqrt{1/P \sum_{p=1}^{P} (\mathrm{rms}_{\sigma_p} - \overline{\mathrm{rms}_\sigma})^2}$ with $\overline{\mathrm{rms}_\sigma} = 1/P \sum_{p=1}^{P} \mathrm{rms}_{\sigma_p}$

Note: P is the total number of patient ($P = 7$ in this study); S_p is the total number of session for the patient p; RMS is the root mean square. $\mu_{p,s} = 1/3 \sum_{o=1}^{3} T_{p,s,o}$ and $\sigma_{p,s} = \sqrt{1/3 \sum_{o=1}^{3} (T_{p,s,o} - \mu_{p,s})^2}$ are the mean and the standard deviation of the translations found by the three operators.

TABLE II. Bladder-neck manual registration interoperator IOV, intersession ISIOV, and interpatient IPIOV variabilities in all directions. All values are in millimeters.

Variability	LR	SI	AP
IOV	2.5	2.5	3.5
ISIOV	1.8	1.0	2.0
IPIOV	1.3	0.8	1.5

Note: LR, left–right; SI, superior–inferior; AP, anterior–posterior.

(dashed red line), B (solid green line), and C (dotted blue line). Method B is better than methods A and C. The optimal value of r for method B is 15 mm but the error for neighbor values is only slightly larger. Table III shows the average misalignment vectors MV of the methods A, B, and C calculated on all data using the best r value for each method (20, 15, and 15 mm for method A, B, and C, respectively). No systematic bias has been noticed since MV values are close to zero in every direction for all methods. In LR and AP directions, standard deviations are similar between each method as opposed to the SI direction for which method B has a lower standard deviation. Figure 4 shows the normalized joint histogram h of the absolute value of the misalignment vector $|MV_{p,s}|$ and the absolute value of the misalignment vector normalized by the session interoperator variability $|MV_{p,s}|/\sigma_{p,s}$, for the method B in LR, SI, and AP directions, respectively. 95%, 82%, and 90% of the registration succeed for LR, SI, and AP directions, respectively. In 29% of the studied sessions, the algorithm fails in one direction and in 1.6% in two directions. It never fails in all three directions for the same session. The rate of sessions without failure is 69%.

4. DISCUSSION

The objective of this work was to propose and quantitatively evaluate registration algorithms of 3D-TA-US post-prostatectomy images in order to correct patient setup before RT treatment.

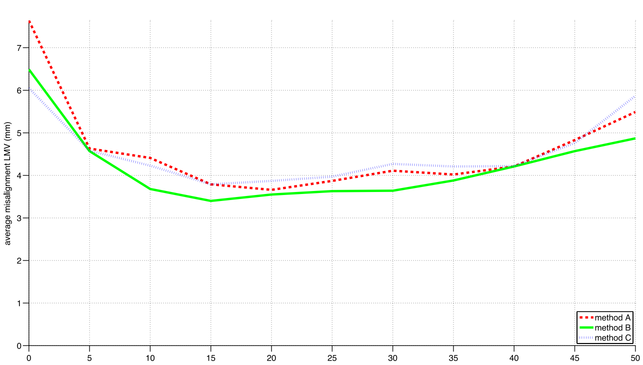

FIG. 3. Average of the misalignment vector lengths LMV as a function of the radius of the ball structuring element used to dilate the RPV. The dashed (red), solid (green), and dotted (blue) lines show the LMV of the methods A, B, and C, respectively. All values are in millimeters.

TABLE III. Average misalignment vector MV of the methods A, B, and C in all directions. All values are in millimeters.

Method (r value)	LR	SI	AP
A (20)	-0.4 ± 1.8	0.2 ± 2.9	-0.3 ± 2.3
B (15)	-0.6 ± 1.7	0.7 ± 2.4	-0.2 ± 2.6
C (15)	-0.4 ± 1.7	0.6 ± 3.7	-0.5 ± 2.4

Note: LR, left–right; SI, superior–inferior; AP, anterior–posterior.

A first issue is registering 3D-TA-US images acquired by manual sweeping of the US probe on the abdominal wall, leading to different field-of-view between images. Moreover, the probe pressure induced by the manual acquisition can deform the tissues and is different between two acquisitions.[36] Secondly, high anatomical variability could occur between sessions. Indeed, even with a strict protocol given to the patient,

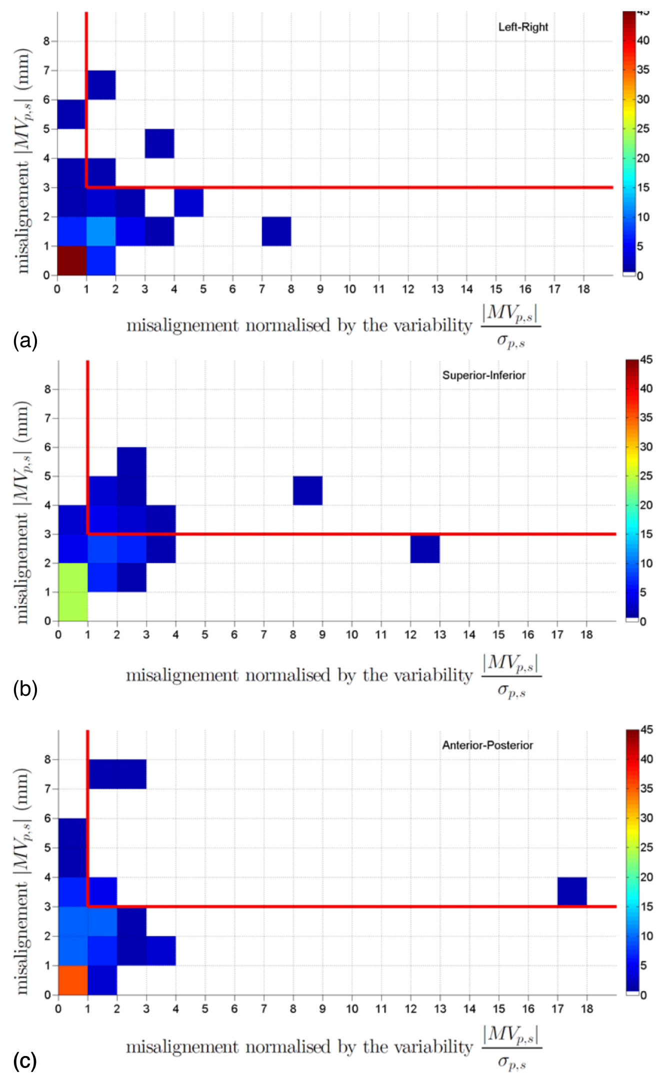

FIG. 4. Normalized joint histogram for the method B of the absolute value of the misalignment vector $|MV_{p,s}|$ and the absolute value of the misalignment vector normalized by the session interoperator variability $\sigma_{p,s}$ in (a) left–right (b) superior–inferior, and (c) anterior–posterior directions. The horizontal and vertical lines (red lines) are the limits above which the registration fails. All values are in millimeters.

it has been observed that the bladder filling varied from one session to the next. For these reasons, two preliminary steps are required before the registration: to compute a mask for the reference and the daily images and to define a ROI on the reference image to only consider the target volume displacement and to restrict the registration on a region that has little anatomical variability. The best size for the dilation of the RPV is of 15 or 20 mm according to the considered method. Lower radii lead to degraded results because not enough image information around the structure of interest is included in the registration. Larger values, or using as ROI the entire conic US mask, also lead to larger registration errors because the anatomical variabilities between the US_{ref} and US_{daily} images are too large. However, the r value does not seem to be a very sensitive parameter since results are close for r values in the range of 10–30 mm. Another difficulty related to the US modality is the presence of speckle noise in the images that differs from one image to the other. It could explain the better results found with method B that includes only gradient information, instead of the two others. On average (Table III), the variabilities of method B are smaller than the interoperator variabilities, which means that the level of precision of the proposed method is of the same order as the manual operators. The two other methods result in superior variabilities compared with the interoperator variability in the SI direction. On the other hand, the accuracy of the patient positioning is difficult to evaluate without a ground truth. Indeed, the reference used in this study is the average of the operators' registrations that is not necessarily a perfect baseline.

Method C which includes gradient and gray value information has been proposed by Kaar *et al.*[25] They compare various similarity measures to register 3D-TA-US/3D-TA-US images acquired on patients who received primary local radiotherapy for a prostate cancer. Using the mutual information by Mattes with the importance images, they find a LMV value of 4.6 ± 1.9 mm to register intersession images. In the present study, the method C leads to a LMV of 3.8 ± 3.0 mm. In addition to the difference of localizations (prostate vs prostatectomy), the reference registration of the two studies are different. Indeed, Kaar *et al.* use the ExacTrac system while in the present study the reference registration is calculated by averaging the manual registration values of three operators.

The use of the importance image (method C), which is a linear combination of the original gray level image, its gradient magnitude image and its Laplacian image, has been proposed by Kaar *et al.* Fifteen linear combinations of these three components have been tested,

$$II_{(w_1,w_2,w_3)} = w_1 I + w_2 \nabla I + w_3 \Delta I \quad \text{with}$$

$$w_i \in \{0, 1/4, 1/2, 3/4, 1\} \, \forall i \in [\![1,3]\!], \sum_{i=1}^{3} w_i = 1,$$

where II, I, ∇I, and ΔI are the importance image, the original image, the gradient image, and the Laplacian image, respectively, and w_1, w_2, and w_3 are the weights related to the images I, ∇I, and ΔI, respectively. The weights equal to $w_1 = 0$, $w_2 = 1$, and $w_3 = 0$ perform the best, which correspond to the method B.

Variations in bladder filling between sessions can affect the algorithm results. When the bladder filling is not sufficient, the contrast between structures such as the bladder neck is drastically degraded and can cause an algorithm failure. Figures 5(a) and 5(b) give an example of bladder filling variation between the reference and the daily 3D-TA-US images. On this pair of images, the algorithm B fails in one direction. This failure corresponds to the point of coordinates (1.5, 6.5) in the LR joint histogram [Fig. 4(a)]. Another cause of failure is the lack of structures of interest in the daily US image. In some cases, the US probe sweep acquisition performed by the radiation therapist is not large enough to capture the entire bladder neck leading to truncating of the bladder neck. Figure 5(d) gives an example of a truncated volume in comparison to the reference image [Fig. 5(c)]. On this pair of images, the algorithm B fails in two directions. This failure corresponds to the points of coordinates (1.5, 4.5) and (1.5, 7.5) in the SI and AP joint histograms, respectively [Figs. 4(b) and 4(c)]. In such cases, a rescanning would have been appropriate.

One limitation of the present study is the absence of quantification of the rotations. As mentioned by Klayton *et al.*[2] and Zhu *et al.*,[37] prostatic bed rotational motion is patient specific but can be quite important in some cases. However, neither the clinical software, which allows only manual translations, nor the treatment couch used in our department is able to take such movements into account. Therefore, rotations cannot be compared to a reference for validation or used to correct patient misalignment. An interesting approach would be to take them into account to improve both the image registration and the patient setup. Likewise, the proposed methodology still needs an expert to manually contour the RPV during the planning process. An interesting prospect would be to automate this step in order to have a fully automatic method rather than a

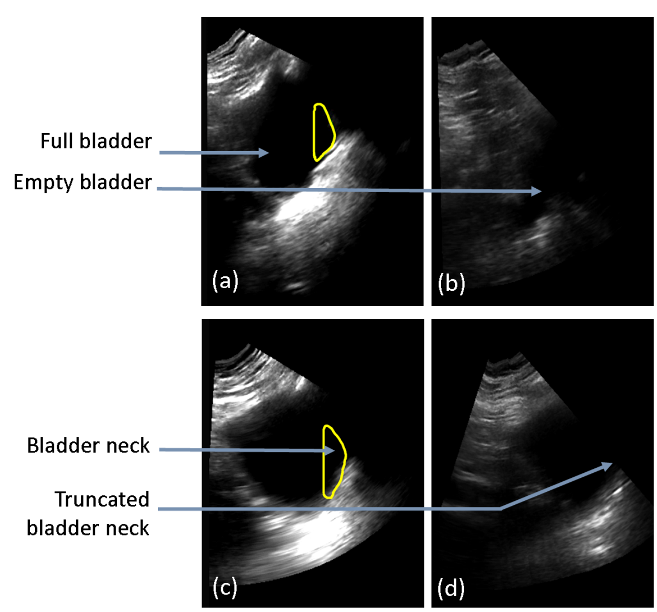

FIG. 5. Example of 3D-TA-US images for which the method B fails. Compared to the US_{ref} image (a), the US_{daily} image (b) is of low quality. Compared to the US_{ref} image (c), the bladder neck of the daily image (d) is truncated. The RPVs contoured on the US_{ref} images are in solid (yellow) line.

semiautomatic one. Automatic segmentation, which is in general a difficult task, has never been investigated on US images in case of prostatectomy patients. One difficulty is linked to the definition of the bladder neck which is ambiguous because it is not an anatomical organ. In contrast, the CTV, which is always manually delineated on the planning CT image for postprostatectomy radiotherapy, even if there is no image guidance, could also be used for registration since the CT image and the reference US image are in the same coordinate system (Fig. 1). Using such a ROI instead of the RPV would probably not change drastically the results since the two volumes encompass almost the same area. However, the results would have been more difficult to compare to the current clinical registration since the latter is done manually by translating the RPV.

Finally, it should be noted that the computation time needed to perform a registration is about 40 s on a single core Intel Xeon CPU E31225 @ 3.10 GHz without any particular optimization. As the algorithm requires a short computation time, it could be used in clinical practice without needing an additional time.

5. CONCLUSION

The proposed semiautomatic registration algorithm based only on gradient information is a reliable approach to setup patients irradiated after a prostatectomy using a US-based IGRT modality. The results of this algorithm have no bias and are in the same variability range as manual registration. As the algorithm requires a short computation time, it could be used in clinical practice provided that a visual review is performed.

ACKNOWLEDGMENTS

This work is supported in part by the Lyric Grant No. INCa-DGOS-4664 and is within the framework of the LABEX PRIMES (ANR-11-LABX-0063) of Université de Lyon, within the program "Investissements d'Avenir" (ANR-11-IDEX-0007) operated by the French National Research Agency (ANR). The authors specially want to thank all radiation therapists who helped them with this study.

[a]Author to whom correspondence should be addressed. Electronic mail: benoit.presles@creatis.insa-lyon.fr

[1]M. Bolla, H. van Poppel, B. Tombal, K. Vekemans, L. Da Pozzo, T. M. de Reijke, A. Verbaeys, J.-F. Bosset, R. van Velthoven, M. Colombel, C. van de Beek, P. Verhagen, A. van den Bergh, C. Sternberg, T. Gasser, G. van Tienhoven, P. Scalliet, K. Haustermans, and L. Collette, "Postoperative radiotherapy after radical prostatectomy for high-risk prostate cancer: Long-term results of a randomised controlled trial (EORTC trial 22911)," The Lancet **380**, 2018–2027 (2012).

[2]T. Klayton, R. Price, M. K. Buyyounouski, M. Sobczak, R. Greenberg, J. Li, L. Keller, D. Sopka, A. Kutikov, and E. M. Horwitz, "Prostate bed motion during intensity-modulated radiotherapy treatment," Int. J. Radiat. Oncol., Biol., Phys. **84**, 130–136 (2012).

[3]W. L. Smith, C. Lewis, G. Bauman, G. Rodrigues, D. D'Souza, R. Ash, D. Ho, V. Venkatesan, D. Downey, and A. Fenster, "Prostate volume contouring: A 3D analysis of segmentation using 3DTRUS, CT, and MR," Int. J. Radiat. Oncol., Biol., Phys. **67**, 1238–1247 (2007).

[4]G. Crehange, C. Mirjolet, M. Gauthier, E. Martin, G. Truc, K. Peignaux-Casasnovas, C. Azelie, F. Bonnetain, S. Naudy, and P. Maingon, "Clinical impact of margin reduction on late toxicity and short-term biochemical control for patients treated with daily on-line image guided IMRT for prostate cancer," Radiother. Oncol. **103**, 244–246 (2012).

[5]T. J. Scarbrough, N. M. Golden, J. Y. Ting, C. D. Fuller, A. Wong, P. A. Kupelian, and C. R. Thomas, "Comparison of ultrasound and implanted seed marker prostate localization methods: Implications for image-guided radiotherapy," Int. J. Radiat. Oncol., Biol., Phys. **65**, 378–387 (2006).

[6]C. F. Serago, S. J. Chungbin, S. J. Buskirk, G. A. Ezzell, A. C. Collie, and S. A. Vora, "Initial experience with ultrasound localization for positioning prostate cancer patients for external beam radiotherapy," Int. J. Radiat. Oncol., Biol., Phys. **53**, 1130–1138 (2002).

[7]S. van der Meer, E. Bloemen-van Gurp, J. Hermans, R. Voncken, D. Heuvelmans, C. Gubbels, D. Fontanarosa, P. Visser, L. Lutgens, F. van Gils, and F. Verhaegen, "Critical assessment of intramodality 3D ultrasound imaging for prostate IGRT compared to fiducial markers," Med. Phys. **40**, 071707 (11pp.) (2013).

[8]P. Chinnaiyan, W. Tomé, R. Patel, R. Chappell, and M. Ritter, "3D-ultrasound guided radiation therapy in the post-prostatectomy setting," Technol. Cancer Res. Treat. **2**, 353–486 (2003).

[9]K. Paskalev, S. Feigenberg, R. Jacob, S. McNeeley, E. Horwitz, R. Price, C. Ma, and A. Pollack, "Target localization for post-prostatectomy patients using CT and ultrasound image guidance," J. Appl. Clin. Med. Phys. **6**, 40–49 (2005).

[10]G. Xiao, J. M. Brady, J. A. Noble, M. Burcher, and R. English, "Nonrigid registration of 3-D free-hand ultrasound images of the breast," IEEE Trans. Med. Imaging **21**, 405–412 (2002).

[11]J. F. Krucker, G. L. le Carpentier, J. B. Fowlkes, and P. L. Carson, "Rapid elastic image registration for 3-D ultrasound," IEEE Trans. Med. Imaging **21**, 1384–1394 (2002).

[12]P. Foroughi and P. Abolmaesumi, "Elastic registration of 3D ultrasound images," in *Medical Image Computing and Computer-Assisted Intervention (MICCAI)* (Springer, Heidelberg, 2005), Vol. 3749, pp. 83–90.

[13]P. Foroughi, P. Abolmaesumi, and K. Hashtrudi-Zaad, "Intra-subject elastic registration of 3D ultrasound images," Med. Image Anal. **10**, 713–725 (2006).

[14]D. Zikic, W. Wein, A. Khamene, D.-A. Clevert, and N. Navab, "Fast deformable registration of 3D-ultrasound data using a variational approach," in *Medical Image Computing and Computer-Assisted Intervention (MICCAI)* (Springer, Heidelberg, 2006), Vol. 4190, pp. 915–923.

[15]C. Leung, K. Hashtrudi-Zaad, P. Foroughi, and P. Abolmaesumi, "Experimental validation of a 4D elastic registration algorithm," in *30th Annual International Conference of the IEEE Engineering in Medicine and Biology Society* (IEEE, Vancouver, British Columbia, 2008), pp. 3961–3966.

[16]S. Khallaghi, C. G. M. Leung, K. Hastrudi-Zaad, P. Foroughi, C. Nguan, and P. Abolmaesumi, "Experimental validation of an intrasubject elastic registration algorithm for dynamic-3D ultrasound images," Med. Phys. **39**, 5488–5497 (2012).

[17]R. Shekhar and V. Zagrodsky, "Mutual information-based rigid and nonrigid registration of ultrasound volumes," IEEE Trans. Med. Imaging **21**, 9–22 (2002).

[18]F. Rousseau, R. Fablet, and C. Barillot, "Robust statistical registration of 3D ultrasound images using texture information," in *International Conference on Image Processing (ICIP), IRISA, Rennes I University France* (IEEE, New York, NY, 2003), Vol. 1, pp. I-581–I-584.

[19]R. Shekhar, V. Zagrodsky, M. J. Garcia, and J. D. Thomas, "Registration of real-time 3-D ultrasound images of the heart for novel 3-D stress echocardiography," IEEE Trans. Med. Imaging **23**, 1141–1149 (2004).

[20]Z. Wang, G. Slabaugh, G. Unal, and T. Fang, "Registration of ultrasound images using an information-theoretic feature detector," in *IEEE International Symposium on Biomedical Imaging (ISBI): From Nano to Macro* (IEEE, Arlington, VA, 2007), pp. 736–739.

[21]J. Woo, B.-W. Hong, C.-H. Hu, K. K. Shung, C.-C. J. Kuo, and P. J. Slomka, "Non-rigid ultrasound image registration based on intensity and local phase information," J. Signal Process. Syst. **54**, 33–43 (2009).

[22]R. J. Schneider, D. P. Perrin, N. V. Vasilyev, G. R. Marx, P. J. del Nido, and R. D. Howe, "Real-time image-based rigid registration of three-dimensional ultrasound," Med. Image Anal. **16**, 402–414 (2012).

[23]R. Wu, K. V. Ling, W. Shao, and W. S. Ng, "Registration of organ surface with intra-operative 3D ultrasound image using genetic algorithm," in *Medical Image Computing and Computer-Assisted Intervention (MICCAI)*, edited by R. E. Ellis and T. M. Peters (Springer, Berlin Heidelberg, 2003), Vol. 2878, pp. 383–390.

[24]V. V. Karnik, A. Fenster, J. Bax, D. W. Cool, L. Gardi, I. Gyacskov, C. Romagnoli, and A. D. Ward, "Assessment of image registration accuracy in three-dimensional transrectal ultrasound guided prostate biopsy," Med. Phys. **37**, 802–813 (2010).

[25]M. Kaar, M. Figl, R. Hoffmann, W. Birkfellner, J. Hummel, M. Stock, D. Georg, and G. Goldner, "Automatic patient alignment system using 3D ultrasound," Med. Phys. **40**, 041714 (7pp.) (2013).

[26]U. Scheipers, S. Koptenko, R. Remlinger, T. Falco, and M. Lachaine, "3-D ultrasound volume reconstruction using the direct frame interpolation method," IEEE Trans. Ultrason. Ferroelectr. Freq. Control **57**, 2460–2470 (2010).

[27]M. Lachaine and T. Falco, "Intrafractional prostate motion management with the clarity autoscan system," Med. Phys. Int. **1**, 72–80 (2013).

[28]P. Poortmans, A. Bossi, K. Vandeputte, M. Bosset, R. Miralbell, P. Maingon, D. Boehmer, T. Budiharto, Z. Symon, A. C. M. van den Bergh, C. Scrase, H. Van Poppel, and M. Bolla, "Guidelines for target volume definition in post-operative radiotherapy for prostate cancer, on behalf of the EORTC Radiation Oncology Group," Radiother. Oncol. **84**, 121–127 (2007).

[29]P. Thévenaz and M. Unser, "Optimization of mutual information for multiresolution image registration," IEEE Trans. Image Process. **9**, 2083–2099 (2000).

[30]J. P. W. Pluim, J. B. A. Maintz, and M. A. Viergever, "Mutual-information-based registration of medical images: A survey," IEEE Trans. Med. Imaging **22**, 986–1004 (2003).

[31]R. Suganya, R. Kirubakaran, and S. Rajaram, "Registration of ultrasound liver images using mutual information technique," in *Computational Intelligence, Cyber Security and Computational Models*, edited by G. Sai Sundara Krishnan, R. Anitha, R. S. Lekshmi, M. Senthil Kumar, A. Bonato, and M. Graña (Springer, India, 2014), Vol. 246, pp. 147–153.

[32]J. P. W. Pluim, J. B. A. Maintz, and M. A. Viergever, "Image registration by maximization of combined mutual information and gradient information," IEEE Trans. Med. Imaging **19**, 809–814 (2000).

[33]S. Klein, J. P. W. Pluim, M. Staring, and M. A. Viergever, "Adaptive stochastic gradient descent optimisation for image registration," Int. J. Comput. Vision **81**, 227–239 (2008).

[34]S. Klein, M. Staring, K. Murphy, M. A. Viergever, and J. P. W. Pluim, "elastix: A toolbox for intensity-based medical image registration," IEEE Trans. Med. Imaging **29**, 196–205 (2010).

[35]L. Ibanez, W. Schroeder, L. Ng, and J. Cates, *The ITK Software Guide*, 2nd ed. (Kitware, Inc., 2005).

[36]M. Fargier-Voiron, B. Presles, P. Pommier, S. Rit, A. Munoz, H. Liebgott, D. Sarrut, and M.-C. Biston, "Impact of probe pressure variability on prostate localization for ultrasound-based image-guided radiotherapy," Radiother. Oncol. **111**, 132–137 (2014).

[37]M. Zhu, S. Bharat, J. M. Michalski, H. A. Gay, W.-H. Hou, and P. J. Parikh, "Adaptive radiation therapy for postprostatectomy patients using real-time electromagnetic target motion tracking during external beam radiation therapy," Int. J. Radiat. Oncol., Biol., Phys. **85**, 1038–1044 (2013).